HOT-WALL SHOCK-WAVE BOUNDARY LAYER INTERACTION OF A COMPLIANT CANTILEVER IN HYPERSONIC FLOW

Dylan D. Dooner[1]**, Nicholas F. Giannelis**[1]**, Andrew J. Neely**[1]

[1]The University of New South Wales, Canberra,
School of Engineering and Technology, Campbell, ACT, 2612, Australia
d.dooner@unsw.edu.au

Keywords: Hypersonics, SBLI, FTSI, aerothermoelasticity, CFD, HyMAX

Abstract: Two-dimensional coupled fluid-structure simulations have been performed using a commercial fluid simulation package to compare the response of a cantilever panel subject to laminar shock-impingement (UNSW's HyMAX) with baseline and elevated wall-temperatures at experimentally comparable flow conditions. This comparison serves as a preliminary study on the value of extending the existing HyMAX case to a heated condition. The thermal state was applied using an isothermal wall with altered elastic modulus and density in the structure. During the simulation, the tip x- and y-deflections, and x- and y-forces were tracked to produce timeseries. These timeseries were then processed using perturbation extraction, and autoregressive power spectral density estimation. Additionally, surface pressure coefficient distributions were extracted. From these results it is shown that the hot case experienced over double the y-force and y-deflection at a lower frequency within the same time-frame. At equivalent deflected states, the hot case experienced 8.4% more y-force when deflected down, and 3.5% less y-force when deflected up. This incremental force variance, coupled with a 28% reduction in elastic modulus and 2.5% reduction in density, leads to the aforementioned significant increase in deflection.

1 INTRODUCTION

The ambition to realise sustained high-speed atmospheric flight is one long held in the field of aeronautics. Advances in numerical methods, computing technologies and understanding of fundamental flow phenomena in recent decades are enabling progress to this end, however, significant challenges persist. The complexities of high-speed numerical flow modelling are well-established in compressible flow literature. [1, 2] Of particular note are the issues associated with the treatment of multiple spatial and temporal scales, extreme environmental conditions, flow discontinuities and turbulent boundary layer fluctuations. These complexities are compounded in the context of multiphysics problems, such as those involving the interaction between a high-speed flow and an elastic structure. The High-Speed Working Group (HSWG) of the Third Aeroelastic Prediction Workshop (AePW-III) was established to assess the state-of-the-art in computational tools for precisely these problems, seeking to establish modelling guidelines for these challenging multiphysics problems. Of specific interest are flows involving pronounced shock wave/boundary layer interaction (SBLI), where the highly nonlinear flow states imply the necessity of high-fidelity aerodynamic modelling; a requirement in contrast to the simplified linear potential methods traditionally favoured by aeroelasticians. While two test cases were considered for the workshop, neither focused specifically on the aerothermal effects experienced by a structure subjected to prolonged high-speed flow environments.

The purpose of the present paper is to assess the experimental merit of extending one of the cases of AePW-III by introducing aerothermal heating of the structure numerically and evaluating the influence on the aeroelastic response. Spatial and temporal variance of the heating response is not considered, merely the elevated state via an analogous isothermal wall. This choice is acceptable given the experimental approach available within the short-duration test (∼200 ms) facility, where the panel must be heated to the desired state immediately prior to experimental run and temperature variations in the structure are negligible during the test window.

2 PROBLEM SPECIFICATION

The University of New South Wales HyMAX (Hypersonic, Multibody Aeroelastic eXperiment) case is one of two cases examined by the HSWG of AePW-III, the other case being the RC19 panel model [3–6]. The UNSW HyMAX case consists of three bodies, hence the multibody term in the acronym. The first body is a 6061-T6 aluminium alloy cantilevered panel with the geometric properties given in Table 1. Material properties are given in Table 2 as extracted from MMPDS-17 [7]. This panel serves as a representative structure of a vehicle control surface. It is supported on the upwind edge by the second body, a 'hammerhead' structure which extends outside the tunnel core-flow. The purpose of the hammerhead is to mitigate three-dimensionality by reducing edge effects of the support.

Table 1: Cantilever geometric properties.

Property	Symbol	Value	Units
Length	**a**	0.130	m
Width	**b**	0.080	m
Thickness	**t**	0.002	m

Table 2: Cantilever material properties.

Property	Symbol	Value [300 K]	Value [623.15 K]	Units	Difference
Density	ρ	2713	2645	$\text{kg} \cdot \text{m}^{-3}$	-2.5%
Elastic Modulus	**E**	69	49.7	GPa	-28%
Poisson's Ratio	ν	0.33	0.33	–	–
Thermal Expansion	α	2.28×10^{-5}	2.28×10^{-5}	K^{-1}	–
Thermal Conductivity	**K**	155.58	155.58	$\text{W} \cdot [\text{m} \cdot \text{K}]^{-1}$	–

Placed above these two bodies is the third body; a shock generator. This shock generator has a $5°$ half-angle and is able to pivot both statically, to set either a $2°$ or $10°$ shock deflection angle, or freely pivot to sweep a dynamic shock across the panel at the generator's free-rotation frequency of 42 Hz. An outline of the geometry is given in Figure 1.
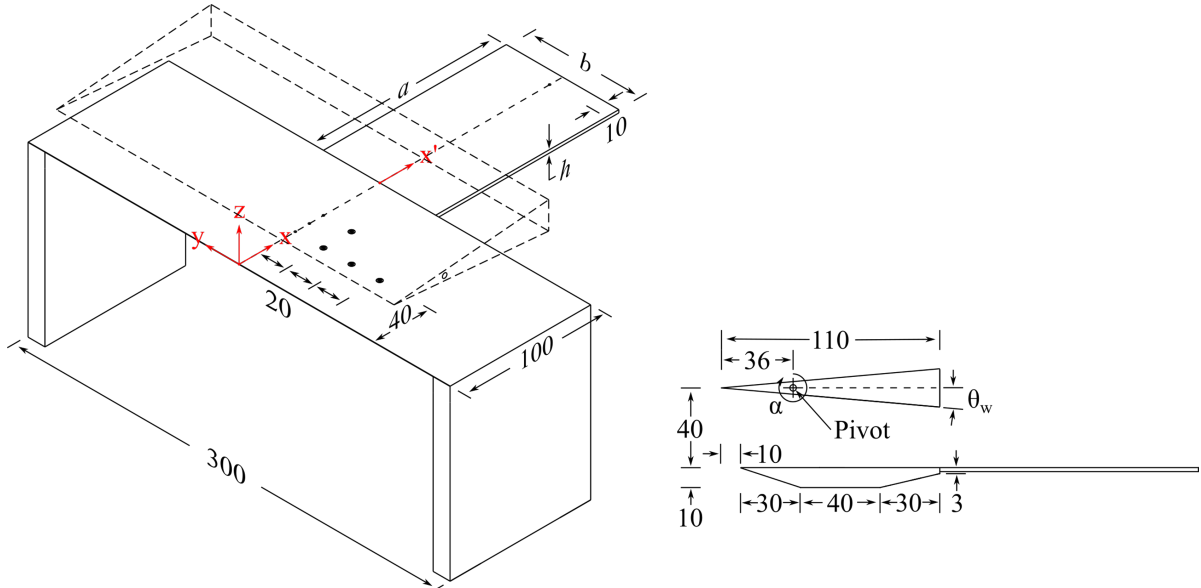
Figure 1: HyMAX geometry.

The test environment for HyMAX is a free-piston compression-heated Ludwieg tube that is located at the University of Southern Queensland (TUSQ). This facility operates by using a high-pressure reservoir to drive a light Nylatron piston down a barrel to heat and compress a charge. This charge is retained by a 100 μm mylar diaphragm until sufficient flow conditions are reached, at which point it ruptures and the charge passes through a converging-diverging nozzle into an evacuated test-section. This produces a free-jet in the test-section allowing for the test to commence. At commencement, by virtue of this developing jet, articles in the test-section are subjected to large, impulsive loads. Once started, the test continues until the core has sufficiently collapsed to no longer envelope the test article. Various flow Mach numbers are achievable with different nozzles. For this experiment. the Mach 6 nozzle was used. This provides approximately 200 ms of quasi-steady flow. Further detailing of the facility is provided in Birch et al. (2018) and Birch et al. (2020). [8, 9]

Freestream properties for each run are determined using isentropic relations, based upon the total pressure history as measured in the nozzle reservoir, and the local ambient temperature and pressure. A summary of the flow conditions used for the HyMAX case is provided in Table 3.

Table 3: HyMAX flow properties.

| Property	Symbol	Value	Units
Freestream Mach	M_∞	5.8	-
Freestream Pressure	P_∞	755	Pa
Total Pressure	P_T	98	kPa
Freestream Temperature	T_∞	75	K
Total Temperature	T_T	578	K
Freestream Density	ρ	0.035	$kg \cdot m^{-3}$
Specific Heat Ratio	γ	1.4	-
Unit Reynolds Number	Re_u	$6.35 \times^{-6}$	m^{-1}

3 METHODOLOGY

For the present work, the $2°$ static shock HyMAX case has been considered. The fluid simulation is performed using the cell-centred, finite volume solver ANSYS Fluent 2023R2® [10]. The two-dimensional, density-based, implicit solver is employed to resolve this high-speed compressible flow. All convective terms are discretised with a second-order upwind scheme, with diffusion terms treated with a second-order central difference. Air is modelled using the ideal-gas equation of state with kinetic-theory defining the dynamic viscosity. Whilst the freestream Mach number may be considered hypersonic, real gas effects are expected to be negligible due to the low total enthalpies generated in the TUSQ facility. As the flow has been demonstrated to be laminar for the $2°$ case, the laminar viscous model has been used.

The aforementioned Unsteady Reynolds-Averaged Navier-Stokes (URANS) simulations were coupled with a large-deflection, Finite Element Model (FEM)-based structural solver within Fluent, producing an 'intrinsic' Fluid-Structure Interaction (FSI) solution. Pressure-farfield conditions were used on most boundary edges, with the downwind boundary being a pressure-outlet. Standard no-slip walls were used for all walls. The thermal boundary condition applied to these walls is static isothermal. Isothermal walls were selected to represent the thermodynamics of the problem, as given the relatively low total temperatures and short test duration, minimal spatial and temporal thermal variation occurs from test-start. For these isothermal walls, two temperatures were considered: a standard 300 K scenario and an elevated wall-temperature of 623.15 K ($350°C$). This elevated temperature was chosen as it has been demonstrated as achievable by in-house experimentation of a carbon-carbon radiative heater and leads to significant mechanical turn-down within the aluminium structure. Data transfer between the fluid-side and structural-side solutions proceeds by parsing of pressure loads only, with viscous forces omitted from the structural solver. Given the pressure differential driven excitation of the HyMAX test case, discussed further in Section 4.1, this approximation appears reasonable, however verification of this assumption remains an avenue of future work.

The mesh used for analysis is a two-dimensional, structured quadrilateral mesh biased to provide refinement around the solid structures. Due to the alignment of the structure with the flow, split leading-edges were used, i.e. no radius was applied. A wall-adjacent cell-height of 1×10^{-5} m was used. 550 cells were used across the length of the panel with 35 cells through its thickness. 450 cells were used across the two long faces of the shock generator, as well as the top, flat edge of the hammerhead. Cumulatively, 450 cells were also used on the bottom three edges of the hammerhead. Total solid cell-count is 15,750 cells and total fluid cell-count is 431,275 leading to a total domain cell-count of 447,025. T. In terms of quality metrics, orthogonality was $0.9949 \pm 0.0107(1\sigma)$, with a skewness of $0.0348 \pm 0.0543(1\sigma)$ and aspect ratio of $23.55 \pm 94.11(1\sigma)$. A visualisation of the mesh is shown in Figure 2. For the aerodynamic force parameters and structural bending, a 2.5D approach is used where the two-dimensional solution is projected through a defined depth. In this case, the defined depth is the panel width.
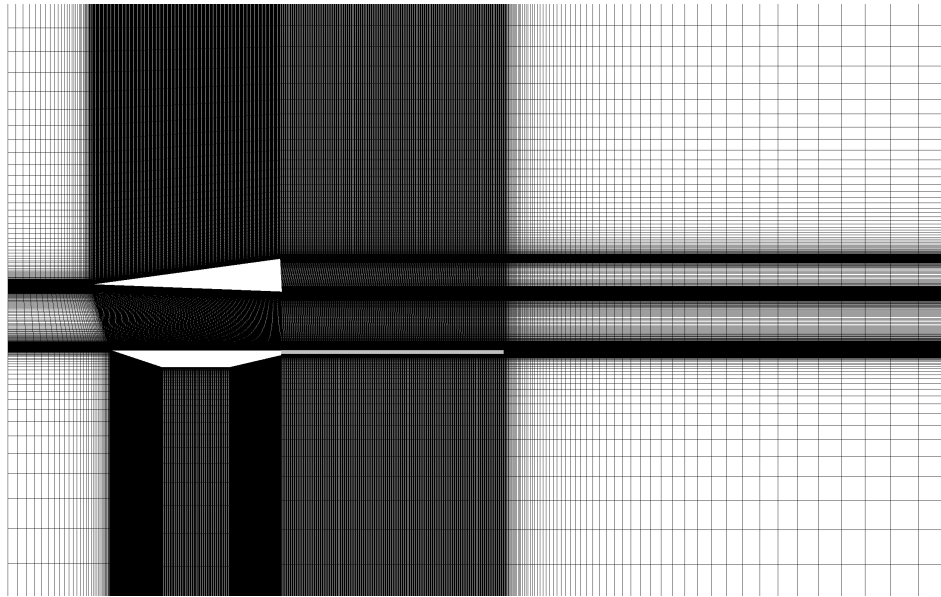
(a) Mesh overview.
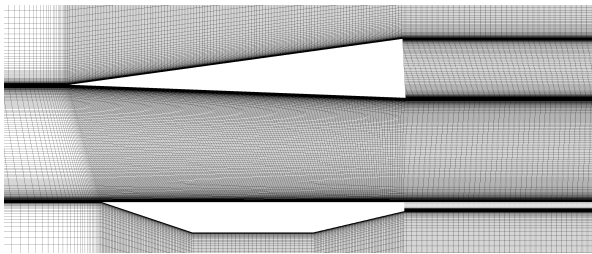
(b) Close-up of near-body mesh.
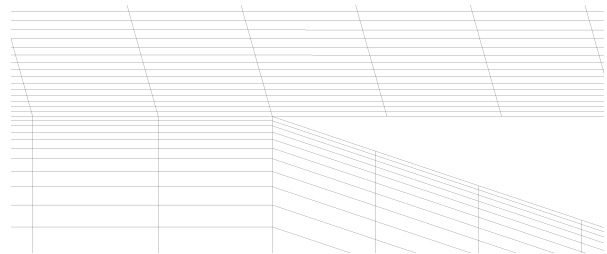
(c) Close-up of hammerhead leading edge.

Figure 2: Mesh overview.

4 ANALYSIS

The analysis is broken into two data summaries. The first are timeseries representations of four quantities of interest: tip y-displacement, tip x-displacement, y-force, and x-force. Both force parameters are computed from a surface pressure integral around the cantilever panel only. The second data summary is spectra of the aforementioned four quantities. Overlaid on the spectra are the natural frequencies of the cantilevered panel system. The first 6 modes for this system under both hot and cold conditions have the modeshapes as given in Figure 3. These are taken from an ANSYS Mechanical® simulation which is a wind-off structural FEM. While the spatial distributions are consistent between the hot and cold panels, the frequencies are not. Both cold and hot frequencies are given in Table 4. As can be seen from the stiffness change there is a $\sim 15\%$ reduction in frequency at the elevated temperature. An important note with these modal results is that the given shapes and frequencies are true as of the real, three-dimensional system. As the simulation was run in two-dimensions, no torsion modes can be represented, and any combined bending-torsion modes will be under-represented.
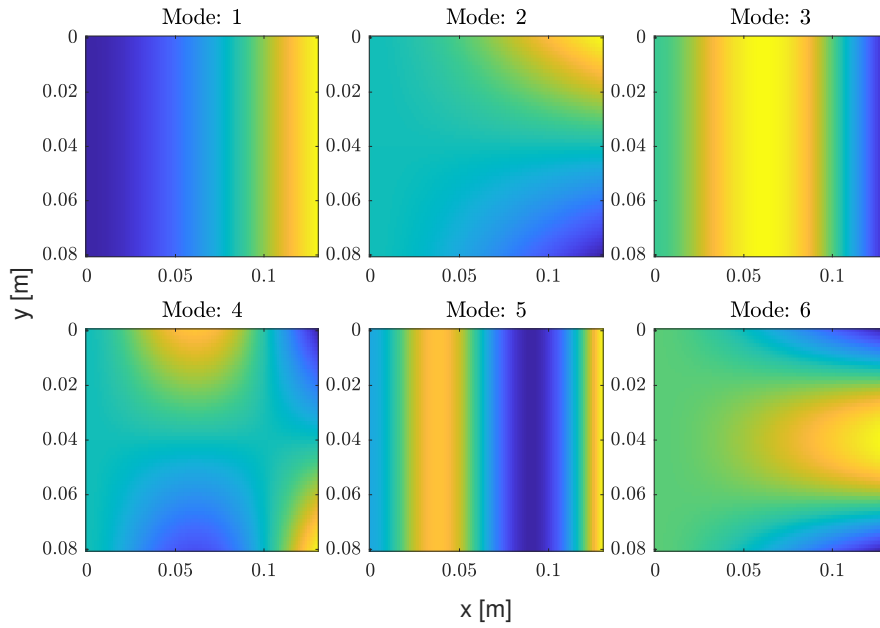
Figure 3: HyMAX hot and cold modeshapes.

Table 4: Cold and hot first 6 modal frequencies.

Case	1 (1B)	2 (1T)	3 (2B)	4 (1C)	5 (3B)	6 (2C)
Cold [Hz]	100	354	623	1,184	1,695	1,883
Hot [Hz]	85	300	528	1,004	1,436	1,596

4.1 Timeseries

The timeseries for the cold and hot panels are provided in Figure 4. Cold results are represented by blue shades and hot by red shades.
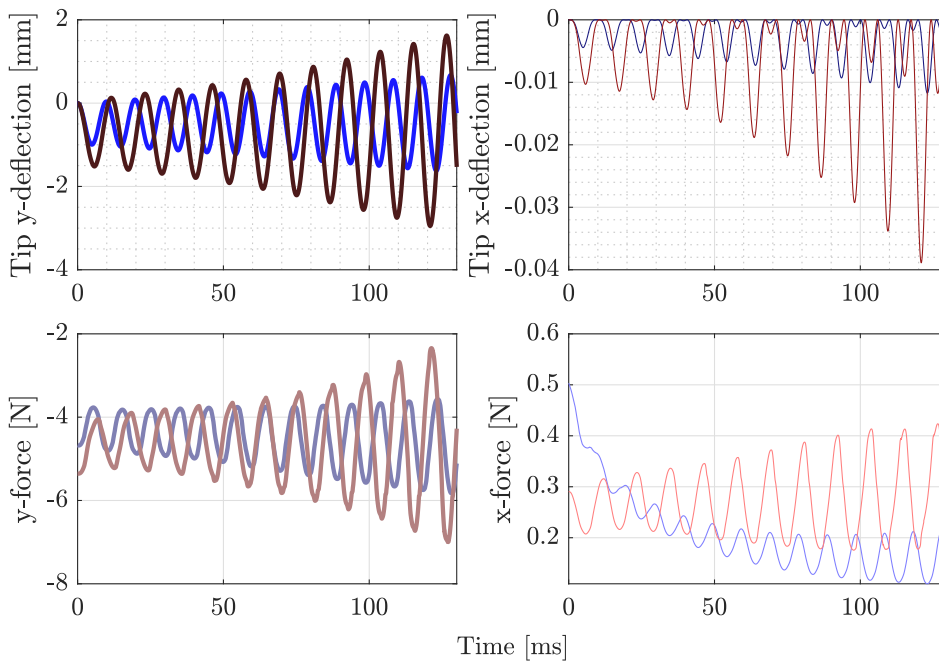

Figure 4: Cold (blue shade) and hot (red shade) timeseries.

6

Generally, the overall behaviours of both cases are analogous. For the y-deflections, both systems are unstable within the given time frame of an experimental run, with consistent amplitude growth cycle to cycle. Additionally, both experience a static deflection downwards, consistent with the shock impingement depressing the structure and gravitational sag. The primary differences between the hot and cold results are the magnitudes of these deflections – the hot is greater in static deflection and oscillatory amplitude, and the frequency of oscillation is higher for the cold case. A comparative summary of the cold versus hot y-deflection offsets (static deflection/neutral state), extrema and amplitudes are presented in Table 5.

Table 5: Tip y-deflection timeseries summary.

Quantity	Cold [mm]	Hot [mm]	Difference [%]
Offset	-0.49	-0.71	44.9
Maxima	0.67	1.80	168.7
Minima	-1.62	-3.10	85.6
Peak Amplitude	1.15	2.45	113.0

The y-deflection behaviours are similarly represented in the x-deflections. A note about the x-deflections, the rectification behaviour observed is both expected and desirable. Whilst the structure is free to stretch, there are no loads significant enough to appreciably stretch the structure. Consequently, if overall length is conserved then when the structure subtends an upwards or downwards deflection arc, it must move backwards (i.e., negative x) in a Cartesian sense.

Insight into the driving dynamics of the hot and cold behaviours are provided by the force timeseries, where the hot case experiences higher aerodynamic loads. Repeating the data presentation as for the y-deflection, the underlying y-force offsets, extrema and amplitudes are given in Table 6.

Table 6: y-force timeseries summary.

Quantity	Cold [N]	Hot [N]	Difference [%]
Offset	-4.49	-4.37	-2.7
Maxima	-3.57	-2.16	-39.5
Minima	-5.83	-7.24	24.2
Amplitude	1.13	2.59	129.2

From the summary tables, the hot system experiences over double the peak y-force and y-deflection amplitude. To understand why this occurs, a deeper analysis into the fluid mechanics is performed by considering the pressure distribution about the panel at three different states in both the cold and hot case. The first state is the initial steady-state fluid system, i.e., t = 0 ms. The second state is a comparison between the maximum cold trough that occurs and the hot trough with the nearest equivalent amplitude. These occur at t = 123 ms for cold and t = 29 ms for hot. The third state is a comparison between the maximum cold peak that occurs and the hot peak with the nearest equivalent amplitude. These occur at t = 128 ms for cold and t = 69 ms for hot. The choice of the maximum cold and equivalent hot states is to assess the fluid with similar structural profiles. This allows for the discrimination of how the flow is different between hot and cold, and how the variation manifests across the upper and lower surfaces of the panel. For example, this permits insight into whether the shock-induced separation bubble dynamics have changed appreciably and whether this change drives the force variation between

the hot and cold cases. Alternatively, this permits an assessment of whether the flow beneath the underside of the panel drives the distinct aeroelastic response characteristics.

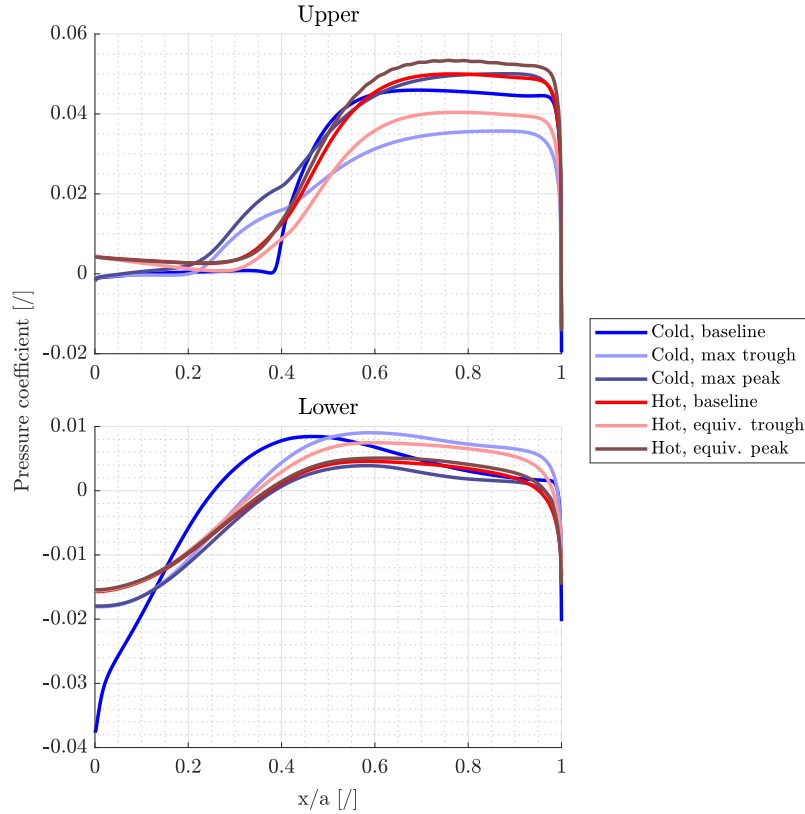The pressure coefficient distributions for these three states under the two cases is presented in Figure 5.

Figure 5: Pressure coefficient distributions.

Assessing collectively, for the upper and lower surfaces there are differences between the hot and cold systems. Considering the baseline initial state, the upper surface when hot has a consistently higher pressure loading. The pressure rise associated with the SBLI is sharper for the cold case but plateaus lower than the hot case. This leads to the hot case having greater suction downwind. Looking at the lower surface, the cold case experiences greater variation of pressure relative to the hot. At the root, the cold is more severely influenced by the expansion fan from the hammerhead, resulting in a 150% larger negative coefficient. This rapidly increases and settles with a similar magnitude to the hot case. The consequence from these two surfaces is that the hot baseline experiences a greater force towards the cantilever's free-end, which drives a larger bending moment favouring greater deflections.

The pattern seen in the baseline state for the upper surface are repeated at both the trough and peak states. The hot case consistently experiences higher downwind suction, driving a larger bending moment. The difference for the trough and peak states are that the cold case experiences an earlier pressure rise closer to the cantilever root and rises at a lower rate than the hot. This distributed pressure rise occurring closer to the root would reduce bending moment. Considering the lower surface results, minimal variation exists between the peak and trough states. In terms of particular values, for the troughs the hot case produces 8.4% more y-force. For the peaks, the hot case produces 3.5% less y-force.

8

In considering these pressure coefficient distributions holistically, it is found that the hot case seemingly alters the shock-wave boundary layer interaction and, with the clear exception at the baseline case, does not appreciably alter the underside of the panel. This altered interaction on the upper surface is therefore the likely driver of the force variation between thermal cases. When coupled with a reduction in elastic modulus, this would lead to the significantly larger deflections observed.

4.2 Spectra

To produce the spectra of the respective cold and hot systems, the signals of the four timeseries' of interest were first detrended. This process aims to remove any bias from the signals, generating the underlying perturbation signal. To do this, an envelope of each signal is taken and the subsequent mean computed based on the upper and lower envelope estimates. By inspection, either a peak-based or RMS-based envelope was used. This was qualitatively assessed based on the resulting perturbation signals, the spectra of the envelope mean signal (was there appreciable spectral corruption), and the spectra of the perturbation signals. Generally, a peak-envelope was used with the cold x-deflection, and hot x-force timeseries benefiting from a RMS-envelope. An example of this detrending and perturbation extraction is shown in Figure 6, where the cold y-deflections are processed using a peak envelope.
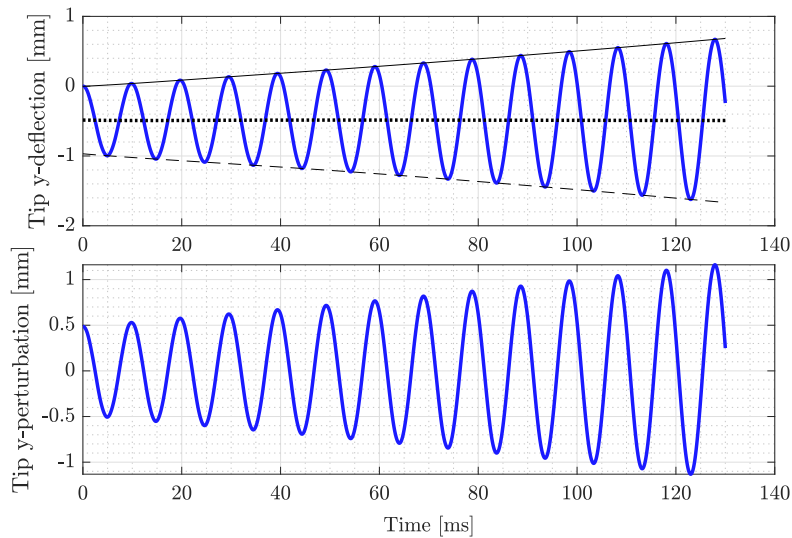

Figure 6: Detrending and perturbation signal of tip y-deflection.

With the detrended signals, an autoregressive (AR) power spectral density (PSD) estimation was performed, as precedence has been set demonstrating its utility in the assessment of short-duration signals, such as those produced from simulation [11–14]. The specific model chosen was the modified covariance method as it is resilient to spectral line-splitting and initial-phase frequency-bias [15]. The order of the model varied between 200 - 800 states and was chosen qualitatively based upon whether the underlying modality of the system was revealed without excessive additional peaks. This screening approach uses prior knowledge of the underlying system dynamics, but does run the risk of screening out dynamics that are unanticipated.

The resultant PSD's from this screening process were then normalised by the maximum signal amplitude to allow for a common figure and to reveal the relative influence of a given frequency component. The results are shown in Figure 7. Overlaid in the same figure are the wind-off natural frequencies of the panel at the two thermal states. These frequencies have been categorised

and presented as either bending, or torsion and combine modes, denoted with a superscript b and t,c respectively. This has been done as the distinction is useful when considering that these results are two-dimensional.
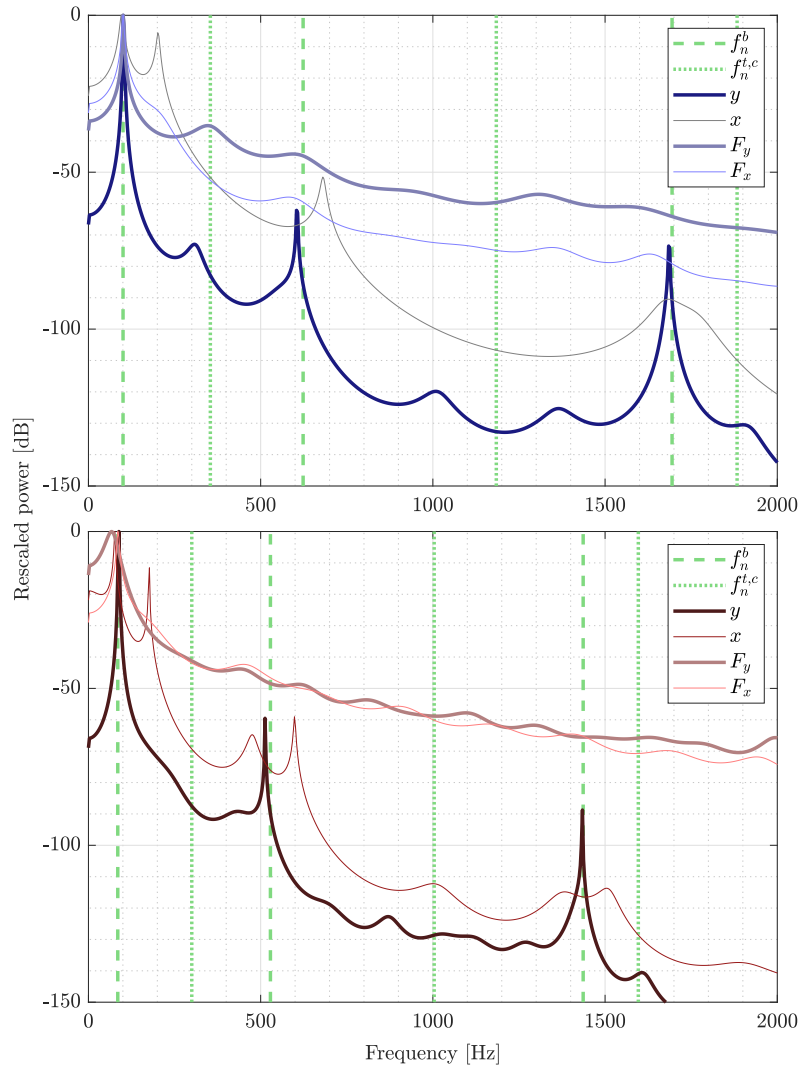

Figure 7: Cold and hot normalised AR-PSD estimates.

Comparable between the hot and cold cases in the tip y-deflection spectra are the modal contributions of the bending modes, expressed clearly by the spectral peaks at those associated frequencies. Minor shifting is occurring, but this is a function of comparing these wind-on results to the wind-off structural frequencies. Dominant modal contribution is clear for first bending across both cases, with the cold case retaining higher mode contribution, i.e., the hot case is more dominated by first-bending. Given the demonstrated increase in the downwind forces on the hot cantilever (i.e., towards the free-edge) as seen in the pressure coefficient distributions, this is expected.

Similar behaviours are again observed for the tip x-deflections, and the x- and y-force spectra. Some peaking is observed around the natural frequencies for the x-deflection results as a consequence of the rectification and the AR-PSD capturing some of these rectification harmonic artefacts. For the y-force, the only clear frequency is that of first-bending for both the cold and

hot cases, with the hot case having reduced peak prominence and hence a higher noise-floor. This is similarly repeated for the x-force results, albeit with a more pronounced distinction between hot and cold results.

5 CONCLUSION

Summarily, a baseline cold (300 K) condition and a secondary hot (623.15 K) condition was assessed by coupled numerical FTSI for the UNSW HyMAX model to explore the value of extending the existing laminar model experimental scope to these heated conditions. The assumed changes would be both structurally, via the change in material properties (notably elastic modulus and density), and aerodynamically, via a changed boundary layer state. Given the shock impingement featured in the model, this changed boundary layer would have a magnified effect.

To assess the effect of heating generally various quantities were obtained. These were Cartesian components of tip-deflection, along with pressure coefficient distributions, and the derived parameters of x- and y-forces. These were assessed in both the time and frequency domain, with the frequency domain using an autoregressive power spectral density approach owing to the short duration of the simulation.

Overall, from the simulations performed it was found that there is a significant change to the amplitude of responses for the hot case, notably y-deflection (113%) and y-force (129%). Regarding the y-deflection, in the frequency domain the modal participation for the hot case are similar to that of the cold case, but with an increased contribution of the first-bending. These changes can be reasonably attributed to the compounding cycle-on-cycle effect of an increased downwind pressure load on the heated cantilever, along with a 28% reduction in elastic modulus.

Ultimately, this simple, preliminary assessment of a heated, laminar HyMAX case has shown an appreciable difference in response without changing the fundamental nature of the case. Consequently, future work will focus on a deeper numerical investigation on this $2°$ laminar case with three-dimensional analysis, as well as investigations into the transitional $10°$ case, and the case with free-oscillation of the shock generator. For future experimental assessment, these results are encouraging and support the development of a heated model tunnel campaign.

6 REFERENCES

[1] Roy, C. J. and Blottner, F. G. (2006). Review and assessment of turbulence models for hypersonic flows. *Progress in Aerospace Sciences*, 42(7–8), 469–530. ISSN 0376-0421. doi:10.1016/j.paerosci.2006.12.002.

[2] Morton, S. A. and Cummings, R. M. (2024). Cfd 2030: Hypersonic modeling &; simulation grand challenge. In *AIAA SCITECH 2024 Forum*. American Institute of Aeronautics and Astronautics. doi:10.2514/6.2024-0683.

[3] Currao, G. M. D., Neely, A. J., Kennell, C. M., et al. (2019). Hypersonic fluid–structure interaction on a cantilevered plate with shock impingement. *AIAA Journal*, 57(11), 4819–4834. ISSN 1533-385X. doi:10.2514/1.j058375.

[4] Talluru, M. K., McQuellin, L. P., and Neely, A. J. (2023). Oscillating shock wave boundary layer interactions on a cantilever plate. In *25th AIAA International Space Planes and Hypersonic Systems and Technologies Conference*. American Institute of Aeronautics and Astronautics. doi:10.2514/6.2023-3094.

[5] Spottswood, S. M., Beberniss, T. J., Eason, T. G., et al. (2019). Exploring the response of a thin, flexible panel to shock-turbulent boundary-layer interactions. *Journal of Sound and Vibration*, 443, 74–89. ISSN 0022-460X. doi:10.1016/j.jsv.2018.11.035.

[6] Brouwer, K. R., Perez, R. A., Beberniss, T. J., et al. (2021). Investigation of aeroelastic instabilities for a thin panel in turbulent flow. *Nonlinear Dynamics*, 104(4), 3323–3346. ISSN 1573-269X. doi:10.1007/s11071-021-06571-4.

[7] Battelle Memorial Institute (2019). *Metallic Materials Properties Development and Standardization*. 14. Battelle Memorial Institute. pp 3-456–3-484.

[8] Birch, B., Buttsworth, D., Choudhury, R., et al. (2018). Characterization of a ludwieg tube with free piston compression heating in mach 6 configuration. In *22nd AIAA International Space Planes and Hypersonics Systems and Technologies Conference*. American Institute of Aeronautics and Astronautics. doi:10.2514/6.2018-5266.

[9] Birch, B., Buttsworth, D., and Zander, F. (2020). Time-resolved stagnation temperature measurements in hypersonic flows using surface junction thermocouples. *Experimental Thermal and Fluid Science*, 119, 110177. ISSN 0894-1777. doi:10.1016/j.expthermflusci. 2020.110177.

[10] ANSYS Inc. (2023). *Fluent 2023 R2: Theory Guide*. ANSYS Inc.

[11] Raveh, D. E. (2004). Identification of computational-fluid-dynamics based unsteady aerodynamic models for aeroelastic analysis. *Journal of Aircraft*, 41(3), 620–632. ISSN 1533-3868. doi:10.2514/1.3149.

[12] Sartor, F. and Timme, S. (2017). Delayed detached–eddy simulation of shock buffet on half wing–body configuration. *AIAA Journal*, 55(4), 1230–1240. ISSN 1533-385X. doi: 10.2514/1.j055186.

[13] Giannelis, N. F. and Vio, G. A. (2021). Influence of turbulence modelling approach on shock buffet computations at deep buffet conditions. In *Proceedings of the AIAA AVIATION 2021 Forum (AIAA Paper 2021-2557)*.

[14] Giannelis, N. F., Thornber, B., and Vio, G. A. (2022). Rigid buffet response of the benchmark supercritical wing for the third aeroelastic prediction workshop. In *Proceedings of the AIAA SciTech 2022 Forum (AIAA Paper 2022-0176)*.

[15] The MathWorks, Inc. (2024). Parametric Methods. Online. Accessed: 28/05/2024. URL; https://au.mathworks.com/help/signal/ug/parametric-methods.html.

[16] PVC (Research Infrastructure), UNSW Sydney (2010). Katana. doi:10.26190/ 669X-A286.

ACKNOWLEDGEMENTS

COPYRIGHT STATEMENT

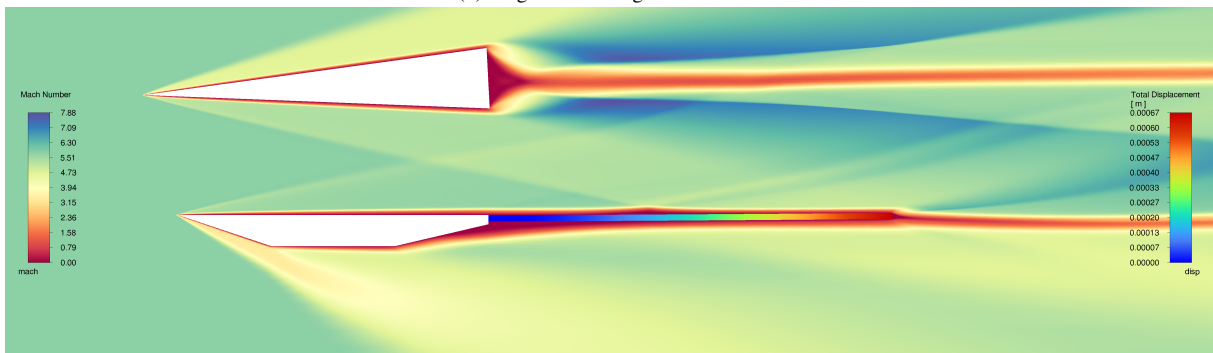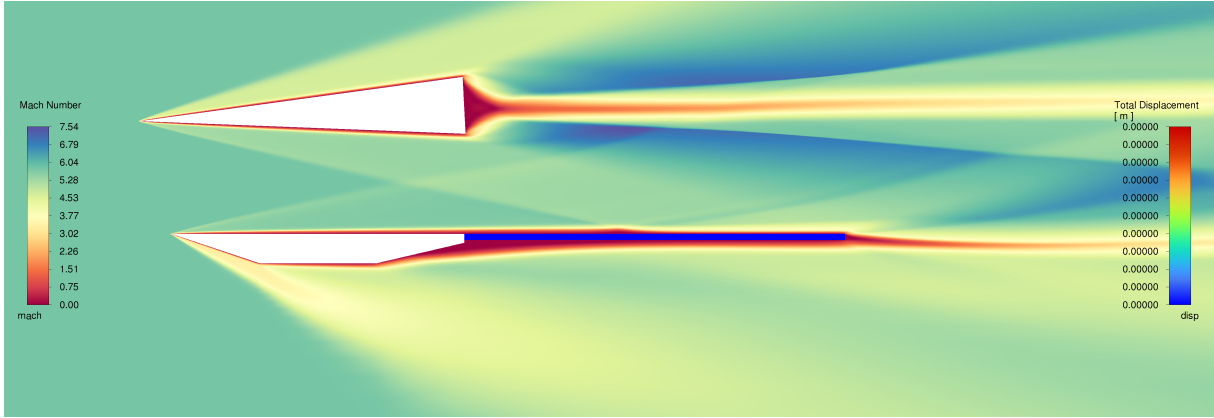**APPENDIX**

(a) Initial cold. t = 0 ms.
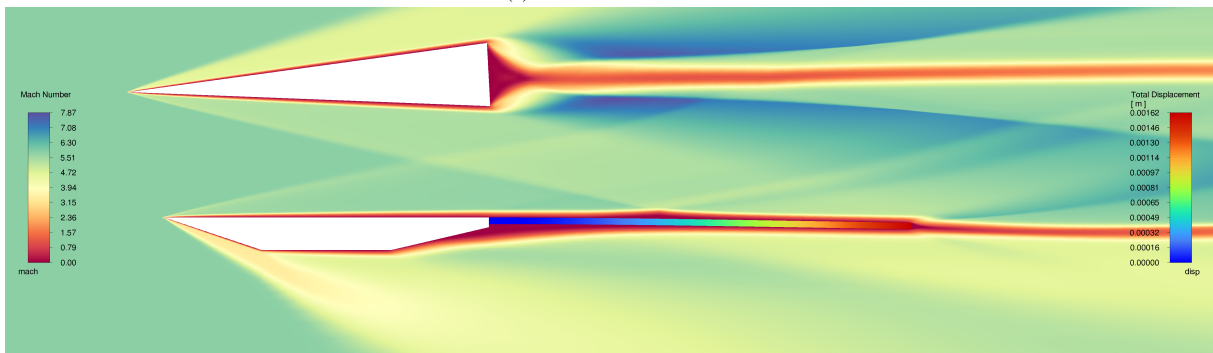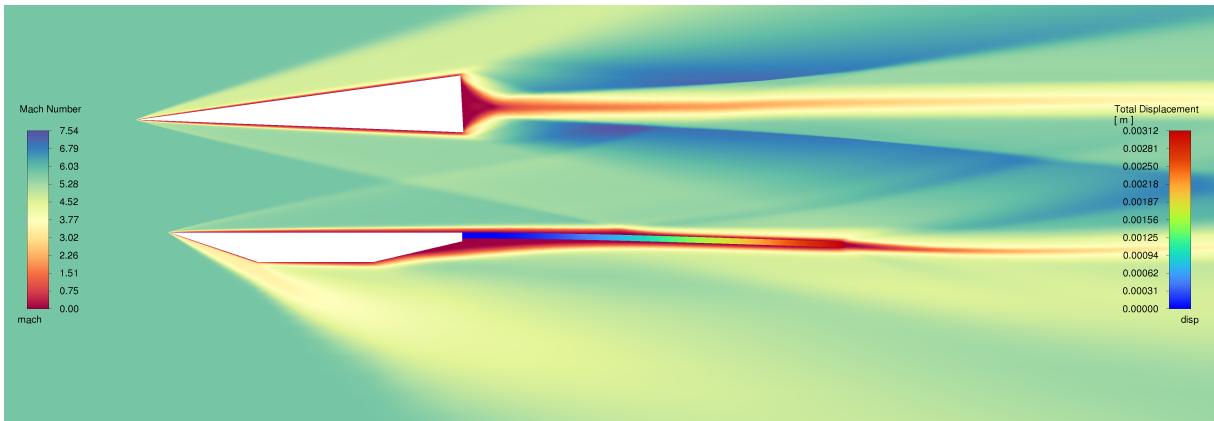

(b) Largest cold trough. t = 123 ms.

(c) Largest cold peak. t = 128 ms.
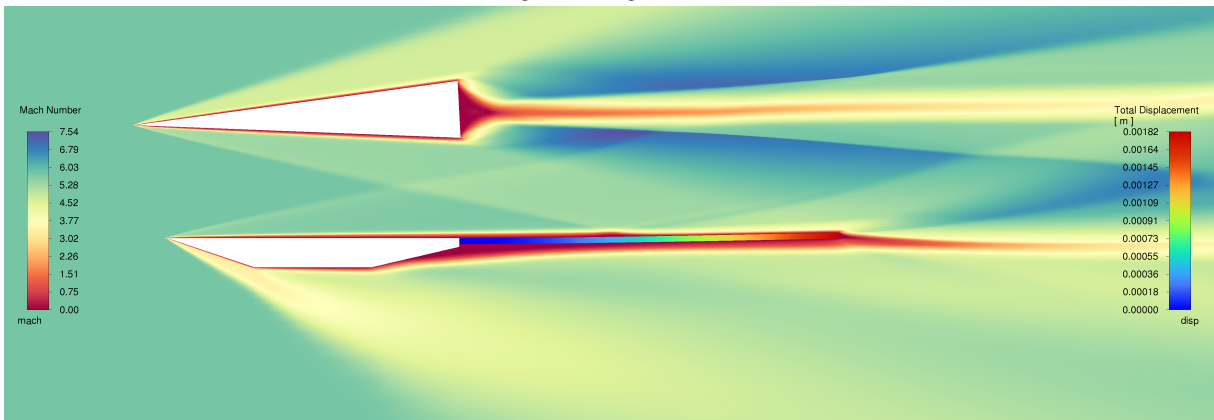
Figure 8: Cold contours evolution.

(a) Initial hot. t = 0 ms.

(b) Largest hot trough. t = 132 ms.

(c) Largest hot peak. t = 138 ms.

Figure 9: Hot contours evolution.